JOURNAL OF SOLID STATE CHEMISTRY **133,** 479–485 (1997)
ARTICLE NO. SC977513

X-Ray and Electron Diffraction Study of the Tetragonal Sodium Tungsten Bronze, $Na_{0.10}WO_3$, with Distorted Perovskite Structure

S. T. Triantafyllou,* P. C. Christidis,*,[1] and Ch. B. Lioutas†

*Laboratory of Applied Physics, and † Department of Solid State Physics, Aristotle University of Thessaloniki, 54006 Thessaloniki, Greece

Received January 24, 1997; in revised form May 30, 1997; accepted June 11, 1997

The crystal structure of the tetragonal sodium tungsten bronze, $Na_{0.10}WO_3$, was investigated by single-crystal X-ray and electron diffraction methods. The average structure has space group $P4/nmm$ and cell constants $a_{av} = 5.2492(5)$ Å, $c_{av} = 3.8953(4)$ Å, and $Z = 2$. The superstructure has space group very probably $P4$ and cell constants $a_s = 7.423(3)$ Å, $c_s = 7.791(1)$ Å, and $Z = 8$. Full-matrix least-squares refinements resulted in a conventional R value of 0.041 [86 observed unique reflections, $I > 2\sigma(I)$] for the average structure and an R value of 0.086 [537 observed unique reflections, $I > 2\sigma(I)$] for the superstructure. The general features of the average structure, which is of distorted perovskite type, are the same as those reported earlier (A. Magnéli, 1951. *Acta Chem Scand.* 5, 670). The two axial bonds of the WO_6 octahedron are not equal (1.95 Å) as observed in the previous work but have significantly different lengths [1.63(6) and 2.27(6) Å]. The superstructure, reported for the first time, results from the average structure by the combined effects of tilting of the WO_6 octahedra about c leading to a doubling of this axis ($c_s = 2c_{av}$) and of shape deformation of these octahedra in the ab plane leading to a supercell in this plane with $a_s = \sqrt{2}a_{av}$.

INTRODUCTION

Although sodium tungsten bronzes, Na_xWO_3 ($0 < x < 1$), have been known since long ago (1), they still attract considerable attention due to their unusual electronic-transport properties (2–5). Their crystal structures were first investigated by Hägg (6), who was able to show that a single cubic phase exists over the large composition range $0.32 < x < 1$. Ribnick *et al.* (7) reported a detailed x–T phase diagram for the composition range $0 < x < 0.5$. These authors established the existence of five phases, which appear in the order monoclinic, orthorhombic, tetragonal I, tetragonal II,[2] and cubic, as x increases from 0 to 0.5. All of these phases, except the tetragonal II phase, are of distorted perovskite type; the tetragonal II phase possesses a distinctly different structure type. It is worth noting that the gradual insertion of Na atoms into the WO_3 array leads to an evolution of structural types similar to that produced by an increase in temperature. Numerous structure investigations have been performed on the various phases of Na_xWO_3 involving X-ray, neutron, and electron diffraction methods. Concerning the tetragonal phases of low sodium content, their structures were first investigated by Magnéli (8, 9) from Weissenberg photographs and visually estimated intensities. This author was able to determine the positions of the tungsten atoms and to describe the general features of the structures, but questions were left as to the accurate positions of the oxygen and sodium atoms and to the correct symmetries, due to the limited accuracy of the measured reflections. A later X-ray study on the tetragonal II phase by Takusagawa and Jacobson (10), performed on the two crystals with compositions $Na_{0.33}WO_3$ and $Na_{0.48}WO_3$, revealed that the WO_6 octahedra host lattice is essentially the same for both crystals and corresponds to the tetragonal potassium tungsten bronze basic structure, commonly referred to as TTB structure type (11). The only difference lies in that the $Na_{0.33}WO_3$ structure appears more distorted than the $Na_{0.48}WO_3$ one, which is also reflected in the corresponding space groups ($P\bar{4}2_1m$ for the first and $P4/mbm$ for the second crystal). In contrast to the tetragonal II phase, no newer analysis has been performed so far on the tetragonal I phase. We therefore considered it to be worthwhile to carry out a detailed structure investigation of this phase with the aim of understanding the properties of the low sodium content phases and the mechanism

[1] To whom correspondence should be addressed.

[2] There is confusion in the literature concerning the designation of the tetragonal sodium tungsten bronzes. In this article the designation of Ribnick (7) is used, according to which the phase with lower Na content is referred to as tetragonal I and the phase with higher Na content as tetragonal II. Magnéli (9a) had previously used a reverse designation, following the chronological order of discovery of these phases.

0022-4596/97 $25.00

of structural phase transitions taking place between them (12).

EXPERIMENTAL

Synthesis and Crystal Growth

The synthesis and growth of single crystals of $Na_{0.10}WO_3$ were performed following the method of Straumanis (13, 14) by reduction of a mixture of Na_2WO_4 and WO_3 with metallic tungsten:

$$3xNa_2WO_4 + (6 - 4x)WO_3 + xW \rightarrow 6Na_xWO_3.$$

The reaction took place in a sealed evacuated silica tube at 1000°C and was complete in about 12 h.

TABLE 1
Crystallographic Data for $Na_{0.10}WO_3$

	Superstructure	Average structure	
	This study	This study	Magnéli (9b)
Space group	*P*4	*P*4/*nmm*	*P*4/*nmm*
a (Å)	7.423(3)	5.2492(5)	5.248
c (Å)	7.791(1)	3.8953(4)	3.895
V (Å^3)	429.3(3)	107.33(2)	107.3
Z	8	2	2
F(0 0 0)	792.8	198.2	
ρ_{cal} (gr·cm^{-3})	7.245		
μ (Mo$K\alpha$) (cm^{-1})	565.5		
Diameter of crystal sphere (mm)	0.19		

X-Ray Diffraction

From powder X-ray diffraction patterns obtained with a modernized Philips PW 1050 diffractometer (Cu$K\alpha$ radiation, Si external standard) it was concluded that the tetragonal I phase (deformed perovskite) was obtained. All the observed peaks could be readily indexed in terms of the cell constants given by Magnéli (9) and no superstructure reflections could be clearly recognized in the pattern. SEM/EDX were used for detecting the amount of Na. The crystals had dark blue color and were of prismatic habit.

For the single-crystal X-ray diffraction study a fairly large crystal was selected, which could be shaped by grinding into a small sphere of 0.19 mm diameter. A preliminary investigation of this crystal by the Buerger precession method showed it to be suitable for such a study. The single-crystal diffractometer used was a modernized Philips PW 1100. All measurements were performed using graphite-monochromated Mo$K\alpha$ radiation and a scintillation counter. The reflection search routine of the diffractometer led to a tetragonal *P* lattice with parameters a_s and c_s related to those of Magnéli (9b), a_{av} and c_{av}, by $a_s = \sqrt{2}a_{av}$ and $c_s = 2c_{av}$. This finding was also confirmed by the electron diffraction study (*vide infra*). It was concluded, therefore, that the structure described by Magnéli (9b) for Na_xWO_3 is only the average one, while the true structure can be described by a supercell with the parameters given above. Accurate cell parameters were obtained by a least-squares fit of the accurate 2θ values of 60 reflections in the region $30.64^\circ < 2\theta < 46.58^\circ$ and are given along with other crystallographic data in Table 1. These parameters do not differ by more than 1 esd from the corresponding ones obtained if triclinic symmetry is assumed. Intensity data were collected for one hemisphere of the reciprocal lattice in the region $5^\circ < 2\theta < 55^\circ$ (scintillation counter, $2\theta/\omega$ scans, 40 steps/reflection increased for α_1–α_2 splitting, step width 0.02°, 0.5–2 sec/step, three standard reflections every 120 min). For better accuracy, every reflection within the above region was measured at least twice. A total of 4365 reflections (excluding standards) were measured, which were further corrected for Lorentz polarization and absorption (spherical crystal) effects. The mean intensity ratio $\langle I/\sigma(I)\rangle$ varied for the different reflection classes between 1 and 15 for the superstructure reflections and between 53 and 127 for the average structure reflections. The internal agreement factor R_{int} of all the intensities was essentially the same (0.069) for the two Laue groups 4/*mmm* and 4/*m*. The same was also true for the average structure reflections ($R_{int} = 0.063$). For the superstructure reflections, the R_{int} factor was 0.177 for 4/*mmm* and 0.170 for 4/*m*. Hence, the Laue group 4/*mmm* was adopted for the average structure, in accordance with Magnéli's assumption, while for the superstructure the possibility for a lower symmetry was left open. By merging the symmetry equivalent reflections (1174 ones) of the average structure, a set of 86 unique reflections were obtained, all of them having $I > 2\sigma(I)$. The only extinction condition observed in this set was *hk*0: $h + k = 2n + 1$, leading unequivocally to the space group *P*4/*nmm*. For the superstructure determination two sets of unique reflections were prepared from the complete set of measured reflections, one set assuming 4/*mmm* as Laue symmetry (337 reflections, 280 observed with $I > 2\sigma(I)$) and another set assuming 4/*m* as Laue symmetry (537 reflections, 427 observed with $I > 2\sigma(I)$). No systematic extinctions were observed for the superstructure reflections.

Electron Diffraction

The electron diffraction study was performed using finely crushed particles of the bulk material glued on copper grids on a Jeol 120CX microscope operating at 120 kV. From the tilting experiments a tetragonal reciprocal space was deduced for the superstructure with lattice parameters $a_s = 7.45$ Å and $c_s = 7.76$ Å, in very good agreement with the values found by X-ray diffraction. Figure 1 shows the ED

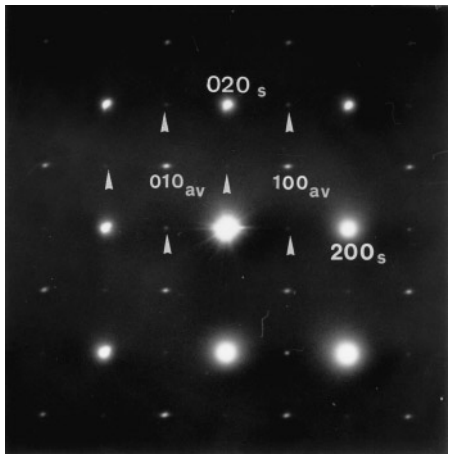

FIG. 1. Electron diffraction patterns along the $[001]_s$ zone axis. Extra weak spots with $h, k = 2n + 1$ indicated by small arrows suggest that there is no systematic extinction condition. Subscripts av and s refer to the average and superstructure tetragonal cell, respectively.

pattern from the $[001]_s$ zone. The main characteristic suggesting the appearance of the superstructure is the presence of weak spots violating the extinction condition $hk0$: $h + k = 2n + 1$ of the $P4/nmm$ space group accepted for the average structure. No systematic extinctions were observed for the superstructure reflections. There are spots $hk0$ with h, $k = 2n + 1$ that are very weak, but the tilting experiments confirm that their appearance is not caused from double diffraction.

STRUCTURE DETERMINATION AND REFINEMENT

Average Structure

Most of the subsequent crystallographic calculations were carried out with the XTAL system of programs (15). Moreover, complex atomic scattering factors taken from (16) were used throughout. The position of the W atom reported by Magnéli (9b) was confirmed in a sharpened Patterson map. The positions of the O atoms could be obtained from a difference Fourier synthesis computed with the refined position of the W atom alone. A full-matrix least-squares refinement based on F_0's and using unit weights and isotropic displacement parameters for all atoms gave $R = 0.057$ ($R_w = 0.069$). Next, anisotropic displacement parameters were introduced, first for the W atom and then for the O atoms, while the weighting scheme $w = 1/\sigma^2(F_0)$ was found as the most appropriate. A difference Fourier synthesis computed at this stage was almost featureless in regions of the unit cell far from the W positions, and only a small spherical peak of 1 e $Å^{-3}$ height appeared at the position 2(*a*) $\frac{3}{4}$, $\frac{1}{4}$, 0 (center of the major perovskite cavity). This peak may be assigned to the Na^+ ion, in accordance with Magnéli's (9b) model. Hence, in the final stage of refinement the Na atom was also introduced at this site with occupancy factor 0.1 and an isotropic displacement parameter equal to the structure's overall one. Due to the very small scattering contribution of the Na atom, its parameters were kept fixed during the refinement. When convergence was reached it was $R = 0.041$, $R_w = 0.048$, GOF = 2.29, and maximum $\Delta p/\sigma(p) = 0.18 \times 10^{-3}$. The residual electron density extrema (-3.1 and 3.0 e $Å^{-3}$) were found near the W position. Atomic positional and displacement parameters of the average structure are given in Tables 2 and 3, and bond lengths and angles are given in Table 4.

TABLE 2
Atomic Positional,[a] Displacement, and Site Occupation Parameters for the Average Structure of $Na_{0.10}WO_3$

		This study					Magnéli (9b)		
Atom		*x*	*y*	*z*	*U*	*pp*	*x*	*y*	*z*
W	2(*c*)	$\frac{1}{4}$	$\frac{1}{4}$	0.4307(2)	0.0187(5)[b]	1	$\frac{1}{4}$	$\frac{1}{4}$	0.435
O1	2(*c*)	$\frac{1}{4}$	$\frac{1}{4}$	1.01(1)	0.08(1)[b]	1	$\frac{1}{4}$	$\frac{1}{4}$	0.935
O2	4(*e*)	0	0	$\frac{1}{2}$	0.074(9)[b]	1	0	0	$\frac{1}{2}$
Na	2(*a*)	$\frac{3}{4}$	$\frac{1}{4}$	0	0.05	0.1	$\frac{3}{4}$	$\frac{1}{4}$	0

[a] The cell origin in this study was taken at center $2/m$ [choice 2 of *International Tables*, Vol. A, Ref. (17)]. Magnéli's atomic coordinates were accordingly transformed for comparison.

[b] These values are equivalent isotropic displacement parameters:

$$U_{eq} = \tfrac{1}{3} \sum_i \sum_j U_{ij}\, a_i^* a_j^* \mathbf{a}_i \cdot \mathbf{a}_j.$$

Superstructure

The starting model for the refinement of the superstructure was derived from the average one, from which some interesting conclusions can be drawn *a priori*. First, the data for the atomic displacement ellipsoids of Table 3 suggest that the most pronounced anisotropy is exhibited by the equatorial O2 atom, which has its major axis perpendicular to the W–O bond direction. This orientation is in agreement with the electron distribution around the O2 site computed from a difference synthesis with isotropically vibrating oxygen atoms. Hence, the tilting of the WO_6 octahedra about the **c** axis should play an important role in the superstructure formation. Second, from the data of Table 3 for the displacement ellipsoid of the W atom it is inferred that no significant deviations of the W atoms from their mean structure positions occur in the superstructure, which implies that these atoms should play a minor role in its appearance.

Concerning the superstructure space group determination it is noticed that, since no extinction condition is observed, no glide plane is expected for the true structure, in contrast to the average one. Moreover, because of the off-center position of the W atoms in the WO_6 octahedra along

TABLE 3
RMS Amplitudes (Å) along the Principal Axes of the Atomic Displacement Ellipsoids for the Average Structure of $Na_{0.10}WO_3$[a]

Atom	RMS amplitudes	*a**	*b**	*c**
W	0.1366	1.0000	0.0000	0.0000
	0.1366	0.0000	1.0000	0.0000
	0.1366	0.0000	0.0000	1.0000
O1	0.1842	0.0000	0.0000	1.0000
	0.3160	0.0000	1.0000	0.0000
	0.3160	− 1.0000	0.0000	0.0000
O2	0.0913	0.7061	0.7061	0.0544
	0.2587	0.0384	0.0384	− 0.9985
	0.3824	− 0.7071	0.7071	0.0000

[a] The direction cosines of the principal axes in terms of the reciprocal crystal axes are also given.

TABLE 4
Interatomic Distances (Å) and Bond Angles (°) for the Average Structure of $Na_{0.10}WO_3$

	This study		Magnéli (9b)
		Symmetry[a]	
W–O1	2.26(6)	(1, 1)	1.95
W–O1	1.63(6)	(1, 2)	1.95
W–O2	1.8754(2)	(1, 1)	1.8726
W–O2	1.8754(2)	(1, 3)	1.8726
W–O2	1.8754(2)	(1, 4)	1.8726
W–O2	1.8754(2)	(1, 5)	1.8726
Na–O1	4 × 2.690	—	2.6362
Na–O2	8 × 2.625	—	2.6899
O1–W–O2	81.72(2)	(1, 1, 1)	82.23
O1–W–O2	81.72(2)	(1, 1, 3)	82.23
O1–W–O2	81.72(2)	(1, 1, 4)	82.23
O1–W–O2	81.72(2)	(1, 1, 5)	82.23
O1–W–O2	98.28(2)	(2, 1, 1)	97.77
O1–W–O2	98.28(2)	(2, 1, 3)	97.77
O1–W–O2	98.28(2)	(2, 1, 4)	97.77
O1–W–O2	98.28(2)	(2, 1, 5)	97.77
O2–W–O2	88.81(1)	(1, 1, 4)	88.95
O2–W–O2	88.81(1)	(1, 1, 5)	88.95
O2–W–O2	88.81(1)	(3, 1, 4)	88.95
O2–W–O2	88.81(1)	(3, 1, 5)	88.95

[a] Symmetry codes: 1, x, y, z; 2, $x, y, z-1$; 3, $\frac{1}{2}-x, \frac{1}{2}-y, z$; 4, $-x, \frac{1}{2}+y, 1-z$; 5, $\frac{1}{2}+x, -y, 1-z$.

the **c** axis, it is concluded that any mirror plane perpendicular to this axis is incompatible with the structure. Hence, the following acentric space groups come into consideration: *P*4, $P\bar{4}$, *P*4*mm*, and $P\bar{4}2m$, all of which are subgroups of the space group *P*4/*nmm*. It is worth noting at this point that the acentricity of the structure is strongly supported by the intensity statistics.

Refinement tests were made for all the aforementioned space groups. In view of the inherent difficulty in refining the O atom positions from X-ray data in the presence of the heavy W atoms, it was found necessary to introduce restraints for the WO_6 octahedra, so that their shapes and dimensions do not deviate considerably from the corresponding ones of the average structure. Also, the refinement strategy was found to be important for the steady convergence of the refinement, because of the presence of strong correlations between certain variables. The alternate refinement of the W and O atoms combined with small damping factors for the parameter shifts was proved most effective. Finally, the unit weighting scheme was found as the most appropriate one in the present case. In the final stage of each refinement model anisotropic displacement parameters were applied for the W atoms and isotropic ones for the O and Na atoms, the latter being kept fixed. The obtained discrepancy factors for only the superstructure reflections, which are more sensitive to the O atom displacements, were 0.207, 0.222, 0.238, and 0.428 for the models *P*4, $P\bar{4}$, *P*4*mm*, and $P\bar{4}2m$, respectively. In view of these values the $P\bar{4}2m$ model can be safely excluded, while for the remaining three models one can notice the following: (*a*) In the *P*4*mm* model all oxygen atoms are forced to lie on mirror planes parallel to **c**, which rules out the possibility of tilting the WO_6 octahedra about this axis. However, such a tilting is supported by the displacement ellipsoids of the oxygen atoms, as was mentioned earlier. Moreover, the agreement of intensities of the symmetry-related reflections slightly favors the first two models, i.e., *P*4 and $P\bar{4}$ (*vide supra*). (*b*) Comparing the models *P*4 and $P\bar{4}$ one observes that in the *P*4 model there are six independent WO_6 octahedra, four of them constrained to the point group symmetry 4 and the remaining two to the point group symmetry 2. On the other hand, in the $P\bar{4}$ model there are only two independent WO_6 octahedra with no symmetry restrictions. Although this latter model seems more flexible, its refinement led to very strongly deformed WO_6 octahedra. Hence, in absence of any other indication from an independent experiment, the *P*4 model was adopted for the true structure of $Na_{0.10}WO_3$. Since in this model the displacement parameters of the axial O atoms (those lying on the 4-fold or 2-fold axes) showed a tendency for steady increase, they were kept fixed and equal to the equivalent isotropic displacement parameter of the axial O1 atom of the average structure. At convergence the maximum $\Delta p/\sigma(p)$ value was 2.18, observed for the U_{22} parameter of W5, while the average $\Delta p/\sigma(p)$ value for the W atoms was 0.28 and the corresponding value for the O atoms was 0.33. The final discrepancy factors obtained were $R = 0.086$ ($R_w = 0.075$) for all the reflections, $R = 0.207$ for only the superstructure reflections, and $R = 0.047$ for only the average structure reflections. The atomic parameters obtained are given in Table 5, while selected bond lengths and angles are given in Table 6.

TABLE 5
Atomic Positional, Displacement and Site Occupation Parameters and Atomic Anisotropic Displacement Parameters for the Superstructure of $Na_{0.10}WO_3$

Atom	x	y	z	U	pp
W1	0	0	0.255(3)	0.011(1)[a]	1
W2	0	0	0.752(3)	0.017(2)[a]	1
W3	$\frac{1}{2}$	0	0.323(3)	0.021(1)[a]	1
W4	$\frac{1}{2}$	0	0.823(3)	0.016(1)[a]	1
W5	$\frac{1}{2}$	$\frac{1}{2}$	0.250(4)	0.079(3)[a]	1
W6	$\frac{1}{2}$	$\frac{1}{2}$	0.759(4)	0.028(2)[a]	1
O11	0	0	0.02(1)	0.08	1
O12	0	0	0.53(1)	0.08	1
O31	$\frac{1}{2}$	0	0.55(1)	0.08	1
O32	$\frac{1}{2}$	0	1.05(1)	0.08	1
O51	$\frac{1}{2}$	$\frac{1}{2}$	0.01(1)	0.08	1
O52	$\frac{1}{2}$	$\frac{1}{2}$	0.52(1)	0.08	1
O13	0.245(5)	−0.038(4)	0.310(5)	0.008(8)	1
O23	0.248(6)	0.031(6)	0.810(8)	0.03(1)	1
O33	0.475(5)	0.261(5)	0.248(6)	0.020(9)	1
O43	0.56(1)	0.275(9)	0.78(1)	0.09(2)	1
Na1	0.25	0.25	0.00	0.05	0.1
Na2	0.25	0.25	0.50	0.05	0.1

Atom	U_{11}	U_{22}	U_{33}	U_{12}	U_{13}	U_{23}
W1	0.011(1)	0.011(1)	0.013(4)	0	0	0
W2	0.019(2)	0.019(2)	0.012(4)	0	0	0
W3	0.014(2)	0.033(2)	0.015(3)	0.000(1)	0	0
W4	0.008(2)	0.023(2)	0.016(3)	−0.000(1)[a]	0	0
W5	0.112(5)	0.112(5)	0.014(6)	0	0	0
W6	0.035(2)	0.035(2)	0.014(4)	0	0	0

[a] These values denote equivalent isotropic displacement parameters:

$$U_{eq} = \tfrac{1}{3} \sum_i \sum_j U_{ij} a_i^* a_j^* \mathbf{a}_i \cdot \mathbf{a}_j$$

TABLE 6
Selected Interatomic Distances (Å) and Bond Angles (°) for the Superstructure of $Na_{0.10}WO_3$[a]

		Symmetry			Symmetry
W1–O11	1.8(1)	(1, 1)	W4–O31	2.12(9)	(1, 1)
–O12	2.1(1)	(1, 1)	–O32	1.75(9)	(1, 1)
–O13	1.89(3)	(1, 1)	–O23	1.89(4)	(1, 1)
–O13	1.89(3)	(1, 2)	–O23	1.89(4)	(1, 9)
–O13	1.89(3)	(1, 3)	–O43	2.12(7)	(1, 1)
–O13	1.89(3)	(1, 4)	–O43	2.12(7)	(1, 9)
W2–O11	2.1(1)	(5, 1)	W5–O51	1.8(1)	(1, 1)
–O12	1.8(1)	(5, 5)	–O52	2.1(1)	(1, 1)
–O23	1.91(4)	(5, 5)	–O33	1.79(4)	(1, 1)
–O23	1.91(4)	(5, 6)	–O33	1.79(4)	(1, 10)
–O23	1.91(4)	(5, 7)	–O33	1.79(4)	(1, 11)
–O23	1.91(4)	(5, 8)	–O33	1.79(4)	(1, 12)
W3–O31	1.77(9)	(1, 1)	W6–O51	2.0(1)	(5, 1)
–O32	2.15(9)	(1, 5)	–O52	1.9(1)	(5, 5)
–O13	1.91(3)	(1, 1)	–O43	1.74(7)	(5, 5)
–O13	1.91(3)	(1, 9)	–O43	1.74(7)	(5, 13)
–O33	2.03(4)	(1, 1)	–O43	1.74(7)	(5, 14)
–O33	2.03(4)	(1, 9)	–O43	1.74(7)	(5, 15)

O11–W1–O13	103(1)	(1, 1, 1)	O31–W4–O23	87(2)	(1, 1, 1)
O12–W1–O13	77(1)	(1, 1, 1)	O31–W4–O43	81(2)	(1, 1, 1)
O13–W1–O13	87(1)	(1, 1, 3)	O32–W4–O23	93(2)	(1, 1, 1)
O11–W2–O23	76(2)	(1, 5, 5)	O32–W4–O43	99(2)	(1, 1, 1)
O12–W2–O23	104(2)	(5, 5, 5)	O23–W4–O43	96(2)	(1, 1, 1)
O23–W2–O23	87(2)	(5, 5, 7)	O23–W4–O43	83(2)	(1, 1, 9)
O31–W3–O13	93(1)	(1, 1, 1)	O51–W5–O33	90(2)	(1, 1, 1)
O31–W3–O33	107(2)	(1, 1, 1)	O52–W5–O33	90(2)	(1, 1, 1)
O32–W3–O13	87(1)	(5, 1, 1)	O33–W5–O33	90(2)	(1, 1, 11)
O32–W3–O33	73(2)	(5, 1, 1)	O51–W6–O43	84(3)	(1, 5, 5)
O13–W3–O33	92(2)	(1, 1, 1)	O52–W6–O43	96(3)	(5, 5, 5)
O13–W3–O33	86(1)	(1, 1, 9)	O43–W6–O43	89(3)	(5, 5, 14)

[a] Symmetry codes:

1, x, y, z;	6, $-x, -y, -z-1$	11, $1-y, x, z$;
2, $-x, -y, z$;	7, $-y, x, z-1$;	12, $y, 1-x, z$;
3, $-y, x, z$	8, $y, -x, z-1$	13, $1-x, 1-y, z-1$;
4, $y, -x, z$;	9, $1-x, -y, z$;	14, $1-y, x, z-1$;
5, $x, y, z-1$	10, $1-x, 1-y, z$	15, $y, 1-x, z-1$

RESULTS AND DISCUSSION

Average X-Ray Structure

A projection of the average structure of $Na_{0.10}WO_3$ along [001] is depicted in Fig. 2, where the selected unit cells for the description of the average structure and the superstructure are also shown. The present study confirmed the model proposed by Magnéli (9b) for $Na_{0.10}WO_3$. The structure is of distorted perovskite type and can be described as a framework of deformed WO_6 octahedra joined by sharing corners, all octahedra being in parallel orientation. The main feature of this structure is the puckered network of the W atoms extending parallel to (001) by being displaced from the octahedra midpoints alternately $\pm 0.270(3)$ Å along [001]. It is worth noting that, while the length of the **c** axis equals the height of a single WO_6 octahedron (which is also the cell constant of the undeformed cubic perovskite WO_3) the a (and b) cell constants are $\sqrt{2}$ times larger, due to the puckering of the W atoms with respect to the ab plane. The main difference of our results in respect to those of Magnéli (9b) concerns the two axial W–O bonds, which in this study were found to have significantly different lengths [1.63(6) and 2.27(6) Å] while in Magnéli's (9b) work they appeared with equal lengths [1.95 Å]. Thus, it is established by this study the existence in the structure of … O–W–O–W … chains running parallel to [001] with alternate short and long lengths.

Superstructure

A projection of the superstructure of $Na_{0.10}WO_3$ along [001] showing two layers of WO_6 octahedra is depicted in

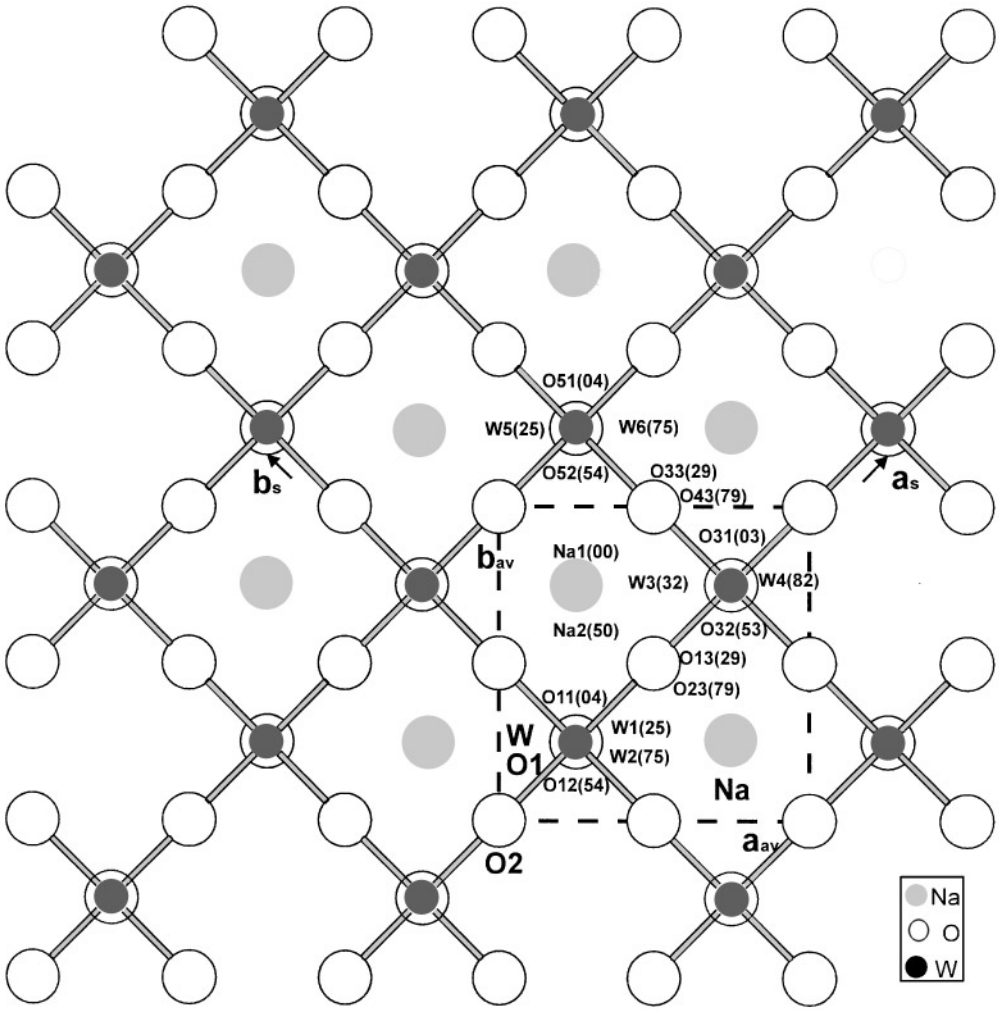

FIG. 2. Normal projection along [001] of the average structure of $Na_{0.10}WO_3$ showing the selected subcell and supercell. The atoms of the asymmetric unit of the average structure are labeled with the larger letters, while the atoms of the asymmetric unit of the superstructure are labeled with the smaller letters.

Fig. 3. It is of interest to compare the true structure of $Na_{0.10}WO_3$ with the structures of orthorhombic (18), monoclinic (19), and triclinic (20) modifications of the pure WO_3, since all of them are of distorted perovskite type with comparable unit cell parameters, i.e., about twice longer than those of the undistorted cubic WO_3 ($a \approx 3.8$ Å).

In WO_3, as in most perovskite-like structures, two principal sets of critical modes appear: (a) the torsional modes giving rise to tilt structures and (b) the deformation modes, which induce distortion of the individual WO_6 octahedra and/or displacement of the W atoms from their central positions (21). Starting from the high-temperature tetragonal phase of WO_3 with the highest symmetry [SG $P4/nmm$, $a_t = 5.25$, $c_t = 3.91$ Å, Ref. (22)], whose octahedra network is identical to that of $Na_{0.10}WO_3$, the transition to the high-temperature orthorhombic phase (SG $Pmnb$, $a_o = 7.341$, $b_o = 7.570$, $c_o = 7.754$ Å) can be explained by freezing a critical mode with normal coordinates parallel to $[010]_t$, which leads to an orthorhombic cell with $a_o = \sqrt{2}a_t$ and $b_o = \sqrt{2}b_t$. Furthermore, a torsional mode gives rise to a tilt structure with $c_o = 2c_t$, the tilt axis being parallel to **a**. The transition from the orthorhombic to the room temperature monoclinic phase (SG $P2_1/n$, $a_m = 7.297$, $b_m = 7.539$, $c_m = 7.688$ Å, $\beta_m = 90.91^\circ$) implies another torsional mode with tilt axis about **c**. Finally, the transition from the monoclinic to the low-temperature triclinic phase (SG $P\bar{1}$, $a_a = 7.309$, $b_a = 7.522$, $c_a = 7.678$ Å, $\alpha_a = 88.81^\circ$, $\beta_a = 90.92^\circ$, $\gamma_a = 90.93^\circ$) involves one additional tilt of the WO_6 octahedra about the **b** axis, the tilting angle being about 17°.

By analogy to the aforementioned phase transitions of WO_3, the derivation of the true structure of $Na_{0.10}WO_3$

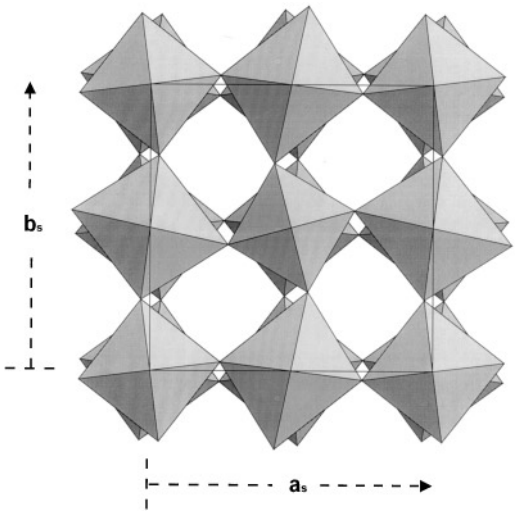

FIG. 3. Normal projection of the supercell contents of $Na_{0.10}WO_3$ along [001]. The tilting of the WO_6 octahedra about the **c** axis, as well as their shape deformation, is clearly seen.

from the average one may be thought of as resulting from the combined effects of rotation and deformation of the WO_6 octahedra. The rotation occurs about the **c** axis and in the opposite sense for successive WO_6 octahedra along [001] (see Fig. 3), giving rise to a doubling of this axis ($c_s = 2c_{av}$). The tilting angles for the different WO_6 octahedra range approximately between 2° and 8°, which implies a maximum shift of the O positions from the corresponding mean structure ones by about 0.27 Å. On the other hand, alternate WO_6 octahedra along the $\langle 110 \rangle_{av}$ directions are deformed in such a way that their point group symmetry degenerates from 4 to 2, the W atoms being negligibly displaced from their mean structure positions. This gives rise to a supercell in the *ab* plane with $a_s = \sqrt{2}a_{av}$.

Concerning the Na atoms, although an ordered distribution of these atoms in the major interstices of the structure cannot be ruled out, it is outside the detection capability of the performed X-ray experiment, due to the very small scattering contribution of these atoms.

In conclusion, it can be said that despite the relatively low accuracy of the derived atomic parameters of the superstructure of $Na_{0.10}WO_3$, especially those of the oxygen atoms, which is due to the aforementioned problems in its refinement, the present study was able to provide the main features of the superstructure and to correlate it with the corresponding average structure.

REFERENCES

1. F. Wöhler, *Ann. Chim. Phys.* **43,** 29 (1823).
2. Ch. J. Raub, A. R. Sweedler, M. A. Jensen, S. Broadstone, and B. T. Matthias, *Phys. Rev. Lett.* **13,** 746 (1964).
3. H. R. Shanks, *Solid State Commun.* **15,** 753 (1974).
4. W. A. Kamitakahara, B. N. Harmon, J. G. Taylor, L. Kopp, H. R. Shanks, and J. Rath, *Phys. Rev. Lett.* **36**, 1393 (1976).
5. R. G. Edgell and G. B. Jones, *J. Solid State Chem.* **81**, 137 (1989).
6. G. Hägg, *Z. Phys. Chem. B* **29,** 192 (1935).
7. A. S. Ribnick, B. Post, and E. Banks, *Adv. Chem. Ser.* **39,** 246 (1963).
8. A. Magnéli, *Arkiv. Kemi* **1,** 269 (1949).
9. (a) A. Magnéli, *Acta Chem. Scand.* **5,** 372 (1951); (b) A. Magnéli, *Acta Chem. Scand.* **5,** 670 (1951).
10. F. Takusagawa and R. A. Jacobson, *J. Solid State Chem.* **18,** 163 (1976).
11. A. Magnéli, *Arkiv. Kemi* **1,** 213 (1949).
12. Ph. Labbe, *Key Eng. Materials* **68,** 293 (1992).
13. M. E. Straumanis, *J. Am. Chem. Soc.* **71,** 679 (1949).
14. E. O. Brimm, J. C. Brantley, J. H. Lorenz, and M. H. Jellinek, *J. Am. Chem. Soc.* **73,** 5427 (1951).
15. S. R. Hall, H. D. Flack, and J. M. Stewart. "XTAL 3.2 Reference Manual." Universities of Western Australia, Geneva, and Maryland, 1992.
16. "International Tables for X-Ray Crystallography," Vol. IV. The Kynoch Press, Birmingham, UK, 1974.
17. "International Tables for Crystallography," Vol. A. Reidel, Dordrecht, 1983.
18. E. Salje, *Acta Crystollogr., Sect. B* **33,** 574 (1977).
19. B. O. Loopstra and P. Boldrini, *Acta Crystallogr.* **21,** 158 (1966).
20. R. Diehl, G. Brandt, and E. Salje, *Acta Crystallogr., Sect. B* **34,** 1105 (1978).
21. E. Salje, *Acta Crystallogr., Sect. A* **31,** 360 (1975).
22. W. Kehl, R. G. Hay, and D. Wahl, *J. Appl. Phys.* **23,** 212 (1952).